

# The Homogeneity of Interstellar Krypton in the Galactic Disk<sup>1</sup>

Stefan I. B. Cartledge

*Department of Physics and Astronomy, Louisiana State University, Baton Rouge, LA 70803*

scartled@lsu.edu

and

David M. Meyer and J. T. Lauroesch

*Department of Physics and Astronomy, Northwestern University, Evanston, IL 60208*

davemeyer@northwestern.edu, jtl@elvis.astro.nwu.edu

## ABSTRACT

We present an analysis of high resolution *HST* Space Telescope Imaging Spectrograph (STIS) observations of Kr I  $\lambda 1236$  absorption in seven sight lines that probe a variety of interstellar environments. In combination with krypton and hydrogen column densities derived from current and archival STIS and *Far-Ultraviolet Spectroscopic Explorer* data, the number of sight lines with reliable Kr/H ISM abundance ratios has been increased by 50% to 26—including paths that sample a range of nearly 5 orders of magnitude in  $f(\text{H}_2)$ , over 2 orders of magnitude in  $\langle n_{\text{H}} \rangle$ , and extending up to 4.8 kpc in length. For sight lines contained entirely within the local spiral arm (the Orion Spur), the spread of Kr/H ratios about the mean of  $\log_{10}[\text{N}(\text{Kr})/\text{N}(\text{H})]_{\text{ISM}} = -9.02 \pm 0.02$  is remarkably tight (0.06 dex), less than the typical datapoint uncertainty. Intriguingly, the only two sight lines that extend through neighboring structures, in particular gas associated with the Carina/Sagittarius Arm, exhibit relatively large, near-solar krypton abundances ( $\log_{10}[\text{N}(\text{Kr})/\text{N}(\text{H})]_{\text{combined}} = -8.75^{+0.09}_{-0.11}$ ). Although these deviations are only measured at the  $2\sigma$  level, they suggest the possibility that krypton abundances beyond the Orion Spur may differ from the local value.

*Subject headings:* ISM: abundances — ultraviolet: ISM

---

<sup>1</sup>Based on observations with the NASA/ESA *Hubble Space Telescope* (*HST*) and the NASA-CNES-CSA

## 1. Introduction

The detection and measurement of absorption features engendered by interstellar krypton became possible with the launch of the *Hubble Space Telescope (HST)* and the Goddard High Resolution Spectrograph (GHRS) in 1990; since that time krypton has garnered significant interest as a direct probe of elemental abundances in the interstellar medium (ISM) and, consequently, of the nature and magnitude of the effects of various interstellar processes. Several factors make krypton particularly useful in this regard. Since krypton is a noble gas with a symmetric electron configuration, essentially all interstellar krypton should be found in the gas phase. Furthermore, since its ionization potential is larger than that of hydrogen, one need only examine resonant absorption features for the neutral form to determine the krypton abundance along a particular sight line. Finally, the intrinsic strengths of the atomic lines and krypton’s low relative abundance to hydrogen combine to place them on the linear portion of the curve of growth for interstellar paths with a wide variety of absorption properties, enabling the accurate measurement of krypton abundances by direct examination of UV absorption features.

GHRS achieved the first reliable detections of interstellar krypton using its unique combination of improved UV sensitivity and spectral resolution with respect to previous instruments (Cardelli et al. 1991). Consequently, Cardelli & Meyer (1997) were able to show that 10 GHRS-observed sight lines probing the local diffuse ISM within about 500 pc possessed nearly identical Kr/H abundance ratios, consistent with the expectation that interstellar krypton is undepleted. Cartledge et al. (2001) broadened the scope of krypton study by presenting Kr/H measurements for seven sight lines observed with both the Space Telescope Imaging Spectrograph (STIS) and the *Far Ultraviolet Spectroscopic Explorer (FUSE)*, including five that intersect translucent clouds. Although these sight lines provided some evidence for enhanced oxygen depletion, no krypton abundance variations distinguishable from measurement uncertainty were apparent, implying a consistent Kr/H ratio for both the diffuse and translucent ISM. The number of sight lines that have been studied to date, however, is still small and samples a limited physical space. In this Letter, we supplement previous krypton abundances derived from GHRS and STIS data with krypton results for seven new sight lines and hydrogen measurements based on STIS and *FUSE* data for nine, increasing the total number with reliable krypton and hydrogen column densities by about 50% to 26. The new sight lines include the first to intersect krypton gas associated with a

---

*Far-Ultraviolet Spectroscopic Explorer (FUSE)*. *HST* spectra were obtained at the Space Telescope Science Institute, which is operated by the Association of Universities for Research in Astronomy, Inc. under NASA contract NAS 5-26555; *FUSE* is operated for NASA by the Johns Hopkins University under NASA contract NAS-32985.

neighboring spiral arm; intriguingly, these sight lines are the only ones to exhibit near-solar Kr/H abundance ratios.

## 2. Observations and Measurements

The current STIS observations of Kr I  $\lambda 1236$  absorption toward seven Galactic O and B stars were garnered through a single *HST* Cycle 8 observing program (GO8241) running from July 1999 until April 2001; a few early results derived from this program were included in the Cartledge et al. (2001) sample. All new krypton spectra were acquired using the E140H echelle grating and  $0.2'' \times 0.2''$  STIS aperture with a  $202\text{\AA}$  spectral window centered at  $1271\text{\AA}$ . Initial processing of the raw data was accomplished using the standard STSDAS STIS data reduction package to produce geometrically corrected two dimensional flat fielded spectra. In the interest of consistency with Cartledge et al. (2001), the Howk & Sembach (2000) scattered-light correction algorithm was then applied to generate one dimensional extracted spectra. In general, Kr I  $\lambda 1236$  absorption appeared in the overlap region between successive spectral orders, which were combined to improve the S/N ratio. The final S/N per pixel values near  $1235\text{\AA}$  ranged from 25–40.

The determination of column densities based on Kr I  $\lambda 1236$  absorption profiles proceeded according to two distinct methods in order to evaluate and correct for uncertainties due to line saturation: profile fitting (Mar & Bailey 1995; Welty, Hobbs, & York 1991) and measurement of apparent optical depth as a function of wavelength (Savage & Sembach 1991). Each method was applied in the same manner and with the same physical constants used by Cartledge et al. (2001); the current results of both profile fitting and apparent optical depth methods are presented in Table 1. Notably, the new column densities derived by each method differ by less than 0.03 dex for an individual sight line, and these results are only up to 0.06 dex larger than values derived under the assumption of no saturation. Since individual measurement uncertainties are of order 0.05–0.11 dex, it is not expected that unresolved saturation is a serious concern for these new sight lines. The results of profile-fitting measurements are adopted for all further analysis and are listed in Table 2, which also summarizes previous GHRS and STIS measurements.

Hydrogen column densities were derived in all cases where Ly- $\alpha$  absorption in the STIS data appeared to be uncontaminated by a stellar contribution and where *FUSE* data existed to provide access to H<sub>2</sub>. STIS spectral orders covering the 1160–1280 $\text{\AA}$  wavelength interval were averaged together to construct an atomic hydrogen absorption profile for each sight line and the associated column density was determined using the continuum-reconstruction method (Bohlin 1975; Diplas & Savage 1994). Notably, four sight lines with newly-measured

hydrogen abundances were examined by Diplas & Savage (1994)—the current H I value agrees with the previous result to within 0.04 dex in each case.

The continuum-reconstruction technique also proved useful in measuring the molecular hydrogen column densities appropriate to several rovibrational absorption profiles apparent in the *FUSE* spectra between 1040 and 1120 Å, since the amount of material present in each sight line was sufficient to generate noticeable damping wings. The *FUSE* LWRS aperture data used to determine molecular hydrogen abundances were collected from several programs examining the ISM, including P101, P116, P235, B030, B071, and Z901. All spectra were processed through CALFUSE, the majority with version 1.8.7. The H I and H<sub>2</sub> values for all 26 sight lines with reliable Kr/H abundance ratios appear in Table 2; however, it should be noted that one of the seven new krypton sight lines, the path toward HD148594, does not appear in the table. The HD148594 STIS spectrum implies an unreasonably large atomic hydrogen column density, likely due to stellar contamination of the Ly- $\alpha$  profile (its spectral type is B8V). The nine new hydrogen column density determinations include the remaining six new sight lines and three that were studied by Cartledge et al. (2001) (HD37903, HD152590, and HD203532), that have subsequently been observed by *FUSE*.

### 3. Local ISM Sight Lines

A striking feature of the tabulated Kr/H abundance ratios is the uniformity of values for sight lines that sample interstellar gas associated only with the local spiral arm, the Orion Spur. This accord is clearly shown in Figure 1, in which the Kr/H abundance ratio is plotted as a function of mean total hydrogen sight line density  $\langle n_{\text{H}} \rangle$ . Although the data set includes sight lines which sample a diverse population of interstellar environments, as indicated by the wide range in properties such as mean density, molecular hydrogen fraction, color excess, direction, and distance (see Table 2 and Figure 2), each datapoint associated with the local arm is consistent with the weighted ISM mean  $\log_{10}(\text{Kr}/\text{H}) = -9.02 \pm 0.02$ . In fact, the spread among sight lines confined to sampling Orion Spur gas, as indicated by the standard deviation of their Kr/H abundance ratios (0.06 dex), is smaller than the typical measurement uncertainty (0.08–0.10 dex). This result is notable, since the observed distribution must include contributions from both intrinsic scatter and measurement error sources. Because these factors are uncorrelated, one must conclude that although the reported errors appear to be somewhat conservative estimates, the tightness of this distribution implies that the homogeneity of the ISM is very narrowly constrained on length scales of a few hundred parsecs. In particular, the observed variation of the interstellar krypton abundance in the Orion Spur can be explained by measurement uncertainty alone.

Similarly uniform gas-phase abundance ratios have been noted for GHRS observations of carbon, nitrogen, and oxygen (Cardelli et al. 1996; Meyer et al. 1997; Sofia et al. 1997; Meyer et al. 1998) in sight lines sampling a range of environments similar to those probed by the krypton sight lines of Cardelli & Meyer (1997). In fact, the abundance ratio scatter in each of the GHRS data sets for these elements and krypton was about 0.06 dex—a surprising result considering that carbon and oxygen are the two elements most abundant in dust while nitrogen and krypton are essentially undepleted in the diffuse ISM (Sofia & Meyer 2001). The addition of several STIS krypton abundance measurements, including values for both longer and denser sight lines, makes a more robust case for the homogeneity of the local ISM, extending the apparent region of its prevalence to several hundred parsecs near the Sun.

One must bear certain caveats in mind, however, when interpreting the significance of the local ISM Kr/H gas-phase abundance ratio uniformity. For instance, the column density quoted for each sight line is integrated along its entire length and thus the quantity Kr/H is a ratio of integrated values. As a result, any low amplitude departures from the mean on relatively small spatial scales are not measurable. But although the degree of increase is in dispute, analytical and numerical models of ISM mixing processes agree that their timescales increase with lengthscale (Roy & Kunth 1995; de Avillez & Mac Low 2002). Hence, the close agreement of hundred-parsec-scale Kr/H ratios indicates that the ISM is generally well-mixed to at least the level of measurement uncertainty, without excluding the possibility of significant small-scale departures (e.g., enrichment). This conclusion is particularly relevant to the two sight lines whose Kr/H abundance ratios diverge from the Orion Spur ISM mean since, by their coincident values, they suggest that the krypton abundances in other spiral arms might be different from the local value.

#### 4. HD116852 and HD152590: Elevated Krypton Abundances?

The sight lines toward HD116852 and HD152590, in addition to each possessing a near-solar Kr/H gas-phase abundance ratio ( $\log_{10}(\text{Kr}/\text{H})_{\odot} = -8.77 \pm 0.07$ ; Anders & Grevesse 1989), share the distinction of extending through gas associated with the Carina/Sagittarius Arm. However, these two paths are widely separated in space from each other and from the bulk of the data set sight lines (see Figure 2). Sembach & Savage (1994) and Sembach & Savage (1996) examined GHRS spectra of HD116852, placing the star at 4.8 kpc (1.3 kpc below the Galactic mid-plane) and identifying eight components comprising three large gas complexes which they associated with local gas and material co-rotating with the Carina/Sagittarius and Norma Arms. The GHRS data contained absorption profiles for several elements, but krypton was not included. Final S/N ratios for the current STIS data do not

approach the values achieved using GHRs, limiting reliable measurement of absorption to the three strongest components. In accord with the Sembach & Savage (1994) summary of the sight line, these absorption features are a blend associated with gas in the Orion Spur and the Carina/Sagittarius Arm.

The study of visual absorption in the HD152590 direction has indicated that this sight line intersects two broad regions of gas spatially coincident with local gas and the Carina/Sagittarius Arm (Raboud et al. 1997). Although the krypton column density for this sight line was previously published by Cartledge et al. (2001), the corresponding hydrogen value was absent. Consequently, it was not possible to distinguish between a large krypton or low oxygen abundance to explain the sight line’s unusual O/Kr gas-phase abundance ratio. Since the first STIS visit to this target, HD152590 has also been observed as a target of the *HST* SNAPSHOT program GO9434. The second spectrum, however, was acquired using a lower resolution setup (the E140M grating centered at 1735Å with  $\Delta v \approx 6.5 \text{ km s}^{-1}$ ). The poorer resolution of this data, coupled with its shorter exposure time and a flex in the continuum near the krypton feature, reduced the quality of krypton abundance measurement significantly, producing the result  $\log_{10} N(\text{Kr})_{\text{HD152590}} = 12.61 \pm 0.11$ . This value is lower than but still consistent with the number in Table 2, and although the complications already noted would likely reduce the apparent krypton abundance, it is possible that the abundance ratio for the HD152590 sight line is less extreme than it currently seems. It should also be noted that since the abundances presented here are integrated values, any apparent gaps between local and distant-spiral-arm Kr/H ratios have been mitigated by local gas in both the HD152590 and HD116852 sight lines.

The krypton enhancements apparent toward HD116852 and HD152590 exist only at the  $2\sigma$  level, but their deviation from the local ISM mean is highlighted by the very tight agreement of Orion Spur sight lines and the coincidence that these two are the only paths to intersect another spiral arm. If they are considered along with the bulk of the sample, the scatter rises only to about the level of datapoint uncertainty and the concept of an homogeneous ISM might conceivably be extended to bridge the inter-arm gaps. However, the agreement between these Kr/H ratios suggests the possibility that the krypton abundance beyond the Orion Spur, in particular in the Carina/Sagittarius Arm, may be measurably different than it is locally. The relevance of such a possibility is demonstrated by the existence of the galactocentric radial abundance gradient ( $-0.07 \text{ dex kpc}^{-1}$  in O/H), that has been identified using stellar atmosphere, H II region, and planetary nebula measurements (Henry & Worthey 1999; Rolleston et al. 2000). The gradient itself, however, is of insufficient magnitude to explain the two atypical krypton ratios. An alternative, that extra krypton could be liberated from dust to raise the gas-phase abundance is belied by the accumulated evidence that krypton is undepleted in the ISM and the lack of any enhancement for strongly

depleted elements in these directions (Cartledge et al. 2003a). Consequently, if these elevated Kr/H ratios are real, it seems that they must be nucleosynthetic in origin.

In this scenario, a potential source can be identified by comparing krypton’s production sites with those of oxygen. As shown in Figure 3 (from Cartledge et al. 2003b), these elements’ abundances are tightly linked. The gas-phase O/Kr ratio departs most dramatically from the ISM mean for the sight lines toward HD116852 and HD152590. Oxygen is predominantly produced in massive star evolution, which also contributes the majority of the krypton nucleosynthesis (Anders & Grevesse 1989). However, a large fraction of the interstellar krypton abundance is derived from the main *s*-process operating in low-mass stars ( $1\text{--}3 M_{\odot}$ ) evolving along the asymptotic giant branch (Raiteri et al. 1993). Consequently, these objects are prime candidates for explaining any krypton enhancement toward HD116852 and HD152590. Notably, this source has recently been cited for the enhancement of other *s*-process elemental abundances. Sofia, Meyer, & Cardelli (1999) examined the interstellar abundances of tin and cadmium and attributed well-determined solar and even supersolar tin abundances to the influence of enrichment by low-to-intermediate mass stars. STIS spectra covering the  $1400.44\text{\AA}$  Sn II line exist for both HD116852 and HD152590, through GO8662 and GO9434 observations, respectively. Unfortunately, the latter spectrum is not of sufficient resolution or S/N to reliably fix the continuum and produce a useful measurement. However, the gas-phase tin abundance toward HD116852 *can* be determined and it is approximately solar ( $\log_{10}(\text{Sn}/\text{H})_{\text{HD116852}} = -9.80 \pm 0.14$ ;  $\log_{10}(\text{Sn}/\text{H})_{\odot} = -9.86$ , Grevesse & Noels 1996). Given its large uncertainty and the possibility that some of the tin in this sight line is depleted from the gas-phase, the HD116852 tin measurement is consistent with the conjecture of main *s*-process enrichment.

## 5. Concluding Remarks

The new krypton abundance measurements presented in this paper supplement earlier results by more fully sampling gas within the Orion Spur and include data from the first sight lines to examine krypton abundances in a neighboring spiral arm. As a result, it has been demonstrated that Kr/H abundance ratios in the local spiral arm ISM are distributed rather tightly about the value  $\log_{10}(\text{Kr}/\text{H}) = -9.02 \pm 0.02$ . The improved coverage of the current data serves to reinforce the conclusion, initially based on previous smaller samples of GHRS krypton, carbon, oxygen, and nitrogen abundance measurements, that the local ISM is very well mixed. Nevertheless, the unusual Kr/H abundance ratios for the sight lines toward HD116852 and HD152590 demonstrate the possibility that small-scale departures exist and are detectable. In fact, the similarity in the krypton abundances for these two

cases and their common property of probing gas outside the local spiral arm suggest that a spatial limit to the efficient mixing of interstellar material may coincide with the boundaries of the Orion Spur. Testing of this speculation will require the acquisition and examination of several additional krypton sight lines with long pathlengths.

In closing, we would like to thank the anonymous referee for his/her comments, and acknowledge the support for this work by STScI through a grant to Northwestern University.

## REFERENCES

- Afflerbach, A., Churchwell, E., & Werner, M. W. 1997, *ApJ*, 478, 190
- Anders, E., & Werner, M. W. 1989, *Geochim. Cosmochim. Acta*, 53, 197
- Biémont, E., & Zeippen, C. J. 1992, *A&A*, 265, 850
- Bohlin, R. C. 1975, *ApJ*, 200, 402
- Cardelli, J. A., & Meyer, D. M. 1997, *ApJ*, 477, L57
- Cardelli, J. A., Meyer, D. M., Jura, M., & Savage, B. D. 1996, *ApJ*, 467, 334
- Cardelli, J. A., Savage, B. D., & Ebbets, D. C. 1991, *ApJ*, 383, L23
- Cartledge, S. I. B., Lauroesch, J. T., & Meyer, D. M. 2003a, in preparation
- Cartledge, S. I. B., Meyer, D. M., Lauroesch, J. T., & Sofia, U. J. 2001, *ApJ*, 562, 394
- Cartledge, S. I. B., Meyer, D. M., & Lauroesch, J. T. 2003b, in preparation
- Chan, W. F., Cooper, G., Guo, X., Burton, G. R., & Brion, C. E. 1992, *Phys. Rev. A*, 46, 149
- de Avellez, M. A., & Mac Low, M.-M. 2002, *ApJ*, 581, 1047
- Diplas, A., & Savage, B. D. 1994, *ApJS*, 93, 211
- Feltzing, S., Holmberg, J., & Hurley, J. R. 2001, *A&A*, 377, 911
- Grevesse, N., & Noels, A. 1996, in *ASP Conf. Proc. 99, Cosmic Abundances*, ed. S. S. Holt & G. Sonneborn (San Francisco: ASP), 116
- Griffen, P. M., & Hutchenson, J. W. 1969, *J. Opt. Soc. Am.*, 59, 1607



- Henry, R. B. C., & Worthey, G. 1999, *PASP*, 111, 919
- Holweger, H. 2001, in *AIP Conf. Proc.* 598, *Solar and Galactic Composition*, ed. R. F. Wimmer-Schweingruber (Berlin: Springer), 23
- Howk, J. C., & Sembach, K. R. 2000, *AJ*, 119, 2481
- Johnson, C. E. 1972, *Phys. Rev. A*, 5, 2688
- Mar, D. P., & Bailey, G. 1995, *Proc. Astron. Soc. Australia*, 12, 239
- Mason, N. J. 1990, *Meas. Sci. Technol.*, 1, 596
- Meyer, D. M., Cardelli, J. A., & Sofia, U. J. 1997, *ApJ*, 490, L103
- Meyer, D. M., Jura, M., & Cardelli, J. A. 1998, *ApJ*, 493, 222
- Meyer, D. M., Jura, M., Hawkins, I., & Cardelli, J. A. 1994, *ApJ*, 437, L59
- Nowak, G., Borst, W. L., & Fricke, J. 1978, *Phys. Rev. A*, 17, 1921
- Raboud, D., Cramer, N., & Bernasconi, P. A. 1997, *A&A*, 325, 167
- Raiteri, C. M., Gallino, R., Busso, M., Neuberger, D., & Käppeler, F. 1993, *ApJ*, 419, 207
- Rolleston, W. R. J., Smartt, S. J., Dufton, P. L., & Ryans, R. S. I. 2000, *A&A*, 363, 537
- Roy, J. -R., & Kunth, D. 1995, *A&A*, 294, 432
- Savage, B. D., & Sembach, K. R. 1991, *ApJ*, 379, 245
- Sembach, K. R., & Savage, B. D. 1994, *ApJ*, 431, 201
- Sembach, K. R., & Savage, B. D. 1996, *ApJ*, 457, 211
- Sofia, U. J., Cardelli, J. A., Guerin, K. P., & Meyer, D. M. 1997, *ApJ*, 482, L105
- Sofia, U. J., & Meyer, D. M. 2001, *ApJ*, 554, L221
- Sofia, U. J., Meyer, D. M., & Cardelli, J. A. 1999, *ApJ*, 522, L137
- Smartt, S. J., Venn, K. A., Dufton, P. L., Lennon, D. J., Rolleston, W. R. J., & Keenan, F. P. 2001, *A&A*, 367, 86
- Vallée, J. P. 2002, *ApJ*, 566, 261
- Wells, W. C., & Zipf, E. C. 1974, *Phys. Rev. A*, 9, 568

Welty, D. E., Hobbs, L. M., & York, D. G. 1991, ApJS, 75, 425

Welty, D. E., Hobbs, L. M., Lauroesch, J. T., Morton, D. C., Spitzer, L., & York, D. G.  
1999, ApJS, 124, 465

Zeippen, C. J., Seaton, M. J., & Morton, D. C. 1977, MNRAS, 181, 527

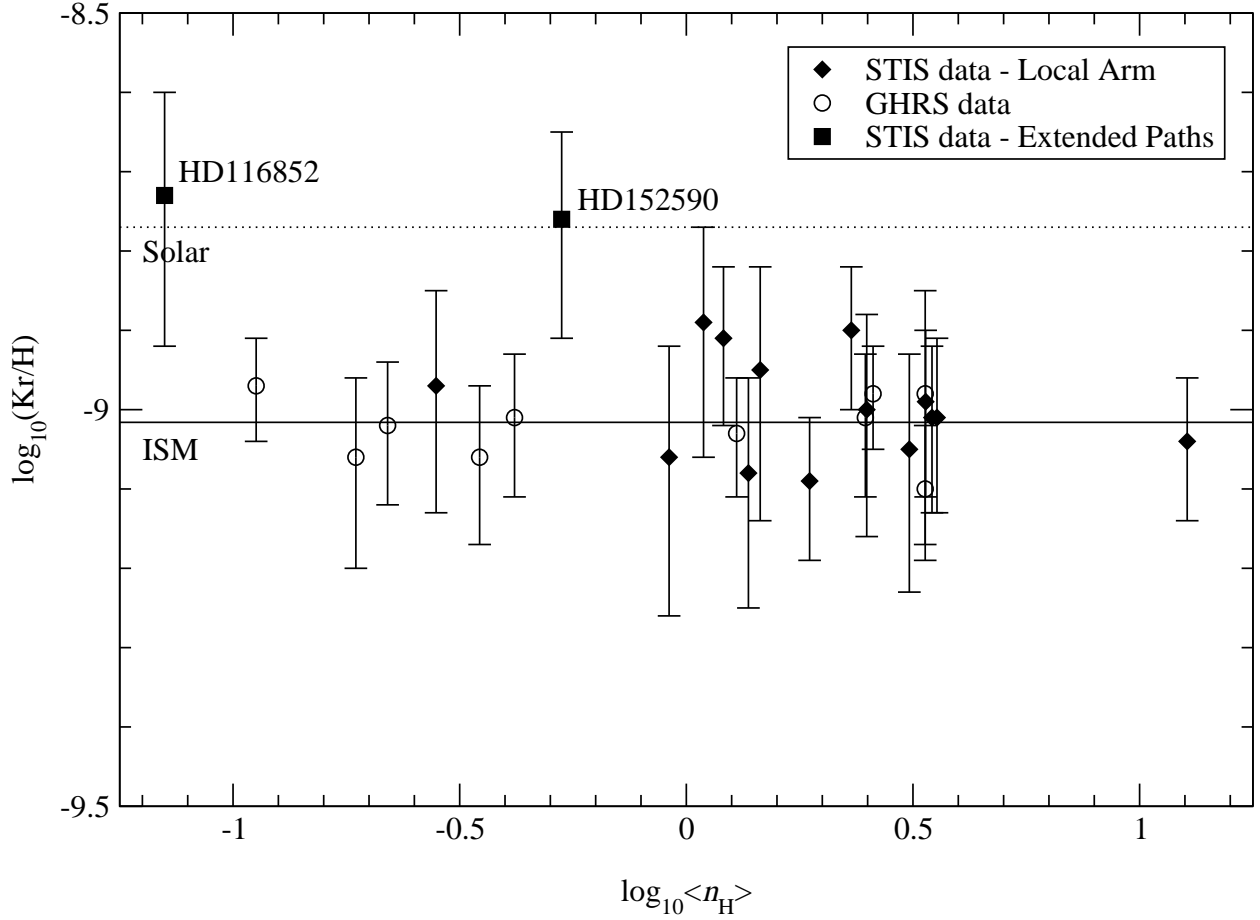


Fig. 1.— Kr/H Abundance Ratios as a Function of Mean Hydrogen Sight Line Density  
Krypton abundances are plotted above as a function of the sight line property  $\langle n_{\text{H}} \rangle$ , which, among the properties listed in Table 2, distinguishes each path most clearly and highlights the fact that there is near-unanimous agreement between each sight line and a single Kr/H within  $1\sigma$  error bars. The only serious detractors from this accord are paths extending through not just local gas, but the Carina/Sagittarius Arm ISM as well.

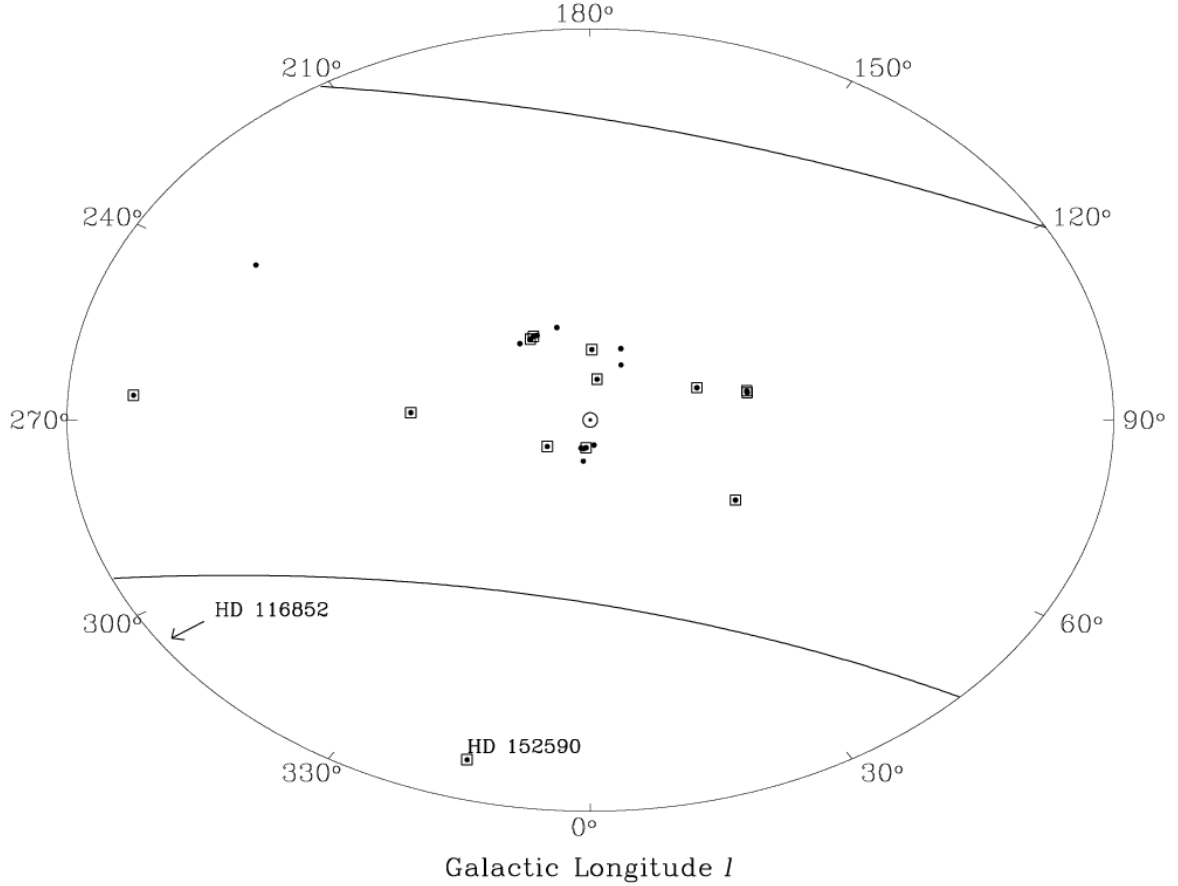


Fig. 2.— STIS and GHRF Sight Lines with Krypton and Hydrogen Abundances  
The positions of stars toward which krypton and hydrogen column densities have been measured by STIS or GHRF and *FUSE* or *Copernicus*, respectively, have been projected onto the Galactic Plane and plotted above in terms of  $l$  and distance; stars observed by STIS are identified by squares. A variety of distances and directions within the Galactic disk are probed by the full data set, yet the only sight lines significantly at odds with a single Kr/H value, those toward HD116852 and HD152590, extend beyond the Carina/Sagittarius Arm. The solid arcs indicate positions for the Carina/Sagittarius (center-ward) and Perseus (anti-center) Arms as described by Vallée (2002); the plot encompasses the Galactic disk within 2 kpc.

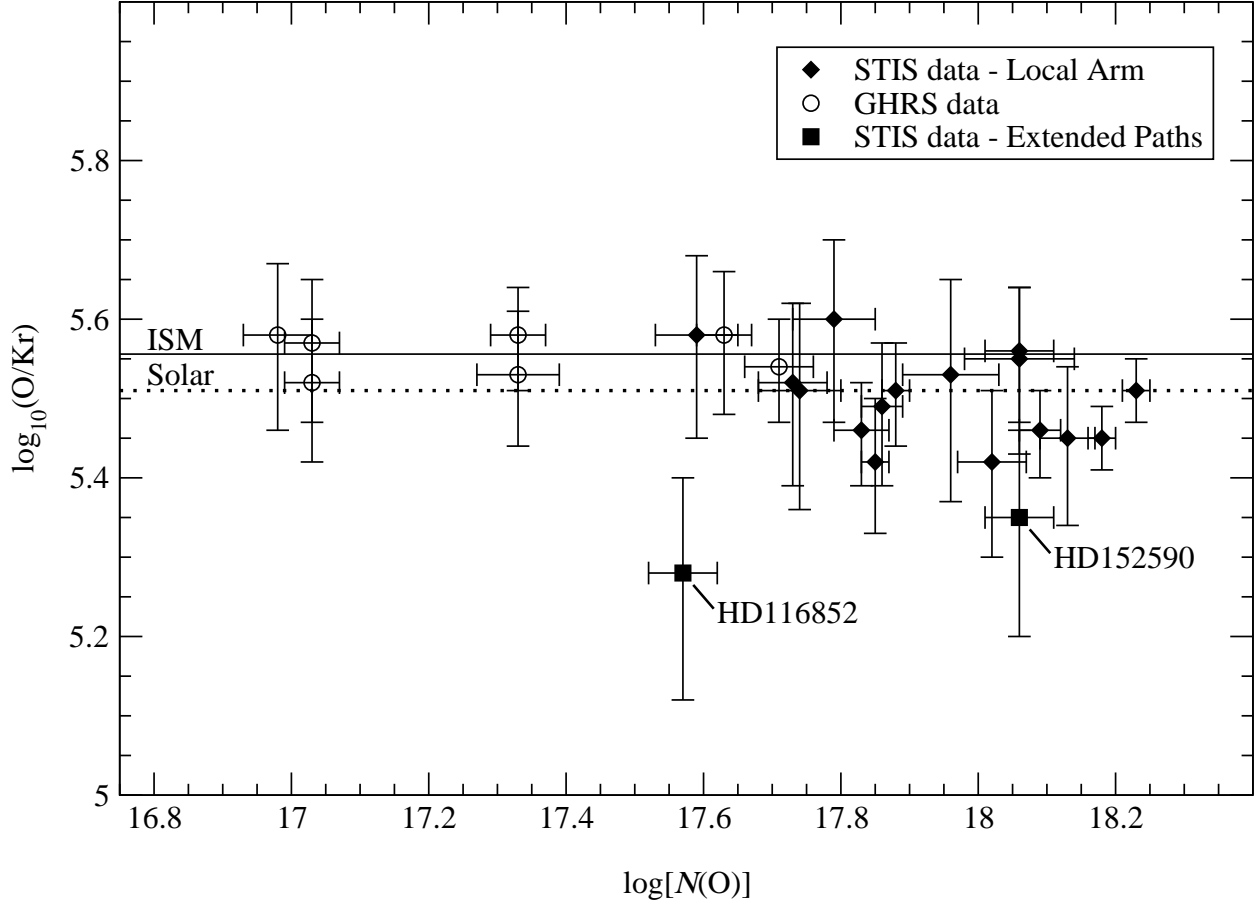


Fig. 3.— O/Kr Abundance Ratios as a Function of Oxygen Column Density

Oxygen-to-krypton abundance ratios are plotted above for sight lines probed using STIS or GHRIS; oxygen data are listed in Cartledge et al. (2003b) and the solar (dotted line) and ISM (solid line) reference levels are derived from Anders & Grevesse (1989), Cardelli & Meyer (1997), Meyer et al. (1998), and Holweger (2000). All sight lines concur with the ISM limit except the HD116852 and HD152590 paths and several with large values of  $\langle n_H \rangle$  that appear to exhibit enhanced oxygen depletion; these datapoints all lie below the line.

Table 1. New Krypton Measurements

Star	Heliocentric Velocities (km s <sup>-1</sup> )	<i>b</i> -values (km s <sup>-1</sup> )	$W_{\lambda 1235}$ (mÅ)	$\log_{10} N(\text{Kr})_A$ (cm <sup>-2</sup> )	$\log_{10} N(\text{Kr})_P$ (cm <sup>-2</sup> )	$\log_{10} N(\text{Kr})$ (cm <sup>-2</sup> )
HD37367	11.5, 16.5	2.3, 2.7	7.81 (0.74)	12.48 (0.04)	12.51 (0.04)	12.51 (0.05)
HD72754	17.1, 20.8, 26.3	1.4, 1.5, 2.7	4.40 (0.79)	12.23 (0.07)	12.23 (0.07)	12.23 (0.10)
HD116852	3.4, 9.7, 15.4	2.1, 1.8, 1.2	5.06 (0.95)	12.29 (0.08)	12.29 (0.08)	12.29 (0.11)
HD148594	-10.5, -4.7	1.6, 2.2	5.73 (0.86)	12.36 (0.06)	12.37 (0.05)	12.37 (0.08)
HD198478	-21.6, -17.3, -12.1, -7.4	2.2, 2.2, 2.0, 1.8	9.80 (1.12)	12.59 (0.05)	12.60 (0.07)	12.60 (0.08)
HD208440	-29.1, -23.1, -17.8, -12.8, -6.3	1.3, 2.5, 1.7, 2.8, 1.4	7.49 (1.58)	12.45 (0.09)	12.43 (0.04)	12.43 (0.10)
HD220057	-16.7, -10.6, -6.3	2.6, 3.0, 3.0	3.93 (0.64)	12.18 (0.07)	12.19 (0.05)	12.19 (0.08)

Note. — The heliocentric velocities and *b*-values listed above specify the cloud component models used to fit the absorption profiles for each sight line. The latter three columns refer to krypton column densities determined by apparent optical depth analysis (subscript *A*) and profile fitting (subscript *P*), followed by the adopted result.

Table 2. Krypton and Hydrogen Sight Line Properties<sup>a</sup>

Star	$E(B-V)$ (mag)	$d_*$ (kpc)	$\log_{10}[N(\text{H I})]$ ( $\text{cm}^{-2}$ )	$\log_{10}[N(\text{H}_2)]$ ( $\text{cm}^{-2}$ )	$\log_{10}[N(\text{H})]$ ( $\text{cm}^{-2}$ )	$\log_{10}[N(\text{Kr})]$ ( $\text{cm}^{-2}$ )	$\log_{10}[\text{Kr}/\text{H}]$	$\log_{10}\langle n_{\text{H}} \rangle$ ( $\text{cm}^{-3}$ )	$\log_{10}f(\text{H}_2)$
HD27778	0.38	0.22	21.10(0.12)	20.72(0.08)	21.36(0.08)	12.37(0.05)	-8.99(0.09)	0.43	-0.34
HD37021	0.54	0.50	21.68(0.12)	...	21.68(0.12)	12.63(0.04)	-9.05(0.12)	0.49	...
HD37061	0.53	0.50	21.73(0.09)	...	21.73(0.09)	12.72(0.03)	-9.01(0.09)	0.45	...
HD37367	0.38	0.36	21.28(0.09)	20.53(0.09)	21.41(0.07)	12.51(0.05)	-8.90(0.08)	0.36	-0.58
HD37903	0.35	0.50	21.16(0.09)	20.85(0.07)	21.46(0.06)	12.37(0.06)	-9.09(0.08)	0.32	-0.31
HD72754	0.33	0.69	21.18(0.12)	20.35(0.10)	21.29(0.10)	12.23(0.10)	-9.06(0.14)	-0.04	-0.64
HD75309	0.21	1.75	21.08(0.09)	20.20(0.12)	21.18(0.08)	12.21(0.09)	-8.97(0.12)	-0.55	-0.68
HD116852	0.21	4.80	20.96(0.09)	19.79(0.11)	21.02(0.08)	12.29(0.11)	-8.73(0.11)	-1.15	-0.93
HD147888	0.51	0.15	21.71(0.09)	20.57(0.15)	21.77(0.08)	12.73(0.03)	-9.04(0.08)	1.07	-0.90
HD152590	0.39	1.80	21.37(0.06)	20.47(0.07)	21.47(0.05)	12.71(0.05)	-8.76(0.11)	-0.28	-0.70
HD185418	0.45	0.69	21.19(0.09)	20.71(0.12)	21.41(0.07)	12.50(0.06)	-8.91(0.09)	0.08	-0.40
HD198478	0.54	0.79	21.32(0.15)	20.87(0.15)	21.55(0.11)	12.50(0.06)	-9.05(0.12)	0.16	-0.38
HD203532	0.29	0.25	21.27(0.09)	20.64(0.08)	21.44(0.07)	12.43(0.08)	-9.01(0.10)	0.55	-0.50
HD207198	0.60	0.62	21.53(0.07)	20.83(0.10)	21.68(0.09)	12.68(0.08)	-9.00(0.12)	0.27	-0.55
HD208440	0.29	0.62	21.23(0.09)	20.29(0.07)	21.32(0.08)	12.43(0.10)	-8.89(0.12)	0.04	-0.73
HD220057	0.23	0.44	21.17(0.09)	20.28(0.07)	21.27(0.07)	12.19(0.08)	-9.08(0.12)	0.14	-0.59
$\zeta$ Per	0.30	0.40	20.81(0.04)	20.67(0.10)	21.20(0.06)	12.17(0.03)	-9.03(0.06)	0.11	-0.23
$\epsilon$ Per	0.11	0.31	20.42(0.06)	19.53(0.15)	20.52(0.06)	11.46(0.07)	-9.06(0.09)	-0.46	-0.68
$\lambda$ Ori	0.12	0.50	20.79(0.08)	19.11(0.11)	20.81(0.07)	11.80(0.05)	-9.01(0.08)	-0.38	-1.40
$\epsilon$ Ori	0.05	0.50	20.46(0.07)	16.57 ...	20.46(0.07)	11.40(0.08)	-9.06(0.10)	-0.73	-3.59
$\kappa$ Ori	0.04	0.50	20.53(0.04)	15.68 ...	20.53(0.04)	11.51(0.07)	-9.02(0.08)	-0.66	-4.55
$\tau$ CMa	0.17	1.51	20.71(0.02)	15.48 ...	20.71(0.04)	11.75(0.05)	-8.97(0.06)	-0.96	-4.93
1 Sco	0.19	0.16	21.21(0.06)	19.23(0.10)	21.22(0.06)	12.24(0.12)	-8.98(0.13)	0.53	-1.69
$\delta$ Sco	0.16	0.16	21.08(0.06)	19.41(0.11)	21.10(0.03)	12.12(0.05)	-8.98(0.06)	0.41	-1.38
$\omega^1$ Sco	0.22	0.23	21.18(0.08)	20.05(0.06)	21.24(0.07)	12.23(0.05)	-9.01(0.08)	0.40	-0.89
$\zeta$ Oph	0.32	0.14	20.71(0.02)	20.65(0.05)	21.15(0.03)	12.05(0.07)	-9.10(0.08)	0.53	-0.20

<sup>a</sup>The sight lines identified by HD numbers were observed with STIS and *FUSE*—the remainder were observed using GHRS and *Copernicus*. In addition to new Kr and H column densities for HD37367, HD72754, HD116852, HD198478, HD208440, and HD220057 and new H results for HD37903, HD152590, and 203532, values are included for the STIS sight lines appearing in Cartledge et al. (2001) and GHRS sight lines compiled by Cardelli & Meyer (1997); the latter have been linearly adjusted to reflect newer  $f$ -values.